- 1 Impact of seamounts on the hydration of subducting plates
- 2 Yuhan Li<sup>1,\*</sup>, Ingo Grevemeyer<sup>1</sup>, Adam H. Robinson<sup>2</sup>, Timothy J. Henstock<sup>2</sup>, Milena
- 3 Marjanović<sup>3</sup>, Anke Dannowski<sup>1</sup>, Norbert Kaul<sup>4</sup>, Ingo Klaucke<sup>1</sup>, Paola Vannucchi<sup>5</sup>,
- 4 Helene-Sophie Hilbert<sup>1</sup>, Damon A.H. Teagle<sup>2</sup>, and Jason Phipps Morgan<sup>6</sup>
- 5 <sup>1</sup>GEOMAR Helmholtz Centre for Ocean Research Kiel, Wischhofstraße 1-3, 24148 Kiel,
- 6 Germany
- <sup>2</sup>School of Ocean and Earth Science, University of Southampton, SO14 3ZH Southampton,
- 8 *UK*
- 9 <sup>3</sup>Institut de Physique du Globe de Paris, Université Paris Cité, CNRS UMR7154, 1 rue
- 10 Jussieu, 75005 Paris, France
- 11 <sup>4</sup>Faculty of Geosciences, University of Bremen, Klagenfurter Straße 2-4, 28359 Bremen,
- 12 *Germany*
- 13 <sup>5</sup>*Università degli Studi di Firenze, 50121 Florence, Italy*
- 14 <sup>6</sup>Barcelona Center for Subsurface Imaging, Institut de Ciéncies del Mar (CSIC), 08003
- 15 Barcelona, Spain
- \* \*Corresponding author, <u>vuli@geomar.de</u>, https://orcid.org/0000-0001-6741-2833

# 17 **ABSTRACT**

18

- The subduction of seamounts greatly affects arc volcanism, earthquakes, and tectonic deformation of the overriding plate, but their role during bending and hydration of the incoming
- 20 plate at subduction zones is poorly understood. Here, we present seismic tomographic results
- 21 along three profiles from the Middle America Trench offshore northern Costa Rica. The crustal

and upper mantle P-wave velocities decrease towards the trench, with the onset of velocity reduction at ~70 km from the trench axis indicating bend-faulting, alteration, and hydration of the incoming plate. The most prominent low velocity anomaly of 7.6-7.8 km/s in the upper mantle occurs beneath a seamount at the outer rise, indicating enhanced hydration with ~2.4 wt% water content, compared to ~1.1-1.3 wt% in the subducting plate away from the seamount. Near the seamount, extremely low heat flow (<10 mW/m²) supports vigorous hydrothermal recharge of seawater. Our results reveal that subducting seamounts efficiently increase the permeability of the oceanic crust prior to subduction, facilitate the migration of seawater into the mantle, exert control on widespread serpentinization and potentially promote water recycling back into the Earth's interior.

## **INTRODUCTION**

Bending of the incoming oceanic plate at deep-sea trenches leads to pervasive fracturing of the lithosphere at the outer rise and outer slope, facilitating hydration of the lithosphere, and eventually governing the transport of water into the Earth's interior (e.g., Peacock, 1990, 2001; Ranero et al., 2003). This process has an important control on the circulation of volatiles (e.g., water, CO<sub>2</sub>) between the hydrosphere and lithosphere. In subduction zones, dehydration of the subducting slab occurs and governs intra-slab intermediate-depth earthquakes (Peacock, 2001) and arc magmatism (Cooper et al., 2020), with the associated hazards; it also fuels deep-sea biological environments (Peacock, 1990). Finally, the amount of the subducted seawater is critical to understanding the Earth's water cycle. The P-wave velocity (Vp) reduction and increase in Vp/Vs from previous wide-angle seismic

(WAS) studies suggest 10-20% of serpentinization occurs in the upper mantle prior to subduction (e.g., Grevemeyer et al., 2007, 2018; Fujie et al., 2016). In contrast, observations from seismic anisotropy indicate a limited average serpentinization of ~6-9% confined to the fault zones (e.g., Miller et al., 2021). It is often assumed that the flux of crustal water is fairly uniform in all subducting oceanic plates, as the quantity of water below topmost crustal layer (layer 2A) is relatively constant. In contrast, the water content in layer 2A is heterogeneous and increases with age up to ~58-70 Ma due to progressive hydrothermal activity (Kardell et al., 2021; Li et al., 2024). However, the global oceanic lithosphere is not uniform in structure, but is instead modulated by potentially 100,000 seamounts (Yu et al., 2024), which can greatly enhance hydrothermal circulation and geochemical exchange on the ridge flanks (Harris et al., 2004). Seamounts can promote hydrothermal circulation across distances >50 km within the oceanic crust (Fisher et al., 2003), leading to mass flux estimates of ~10<sup>14</sup> kg/yr globally, which ultimately affects subseafloor microbial ecosystems (Harris et al., 2004; Hutnak et al., 2008; Fisher & Wheat, 2010). In addition, the loading of volcanic edifices and magmatic intrusions during the building of seamounts deforms the pre-existing oceanic structure (e.g., Watts et al., 1985), creating a structurally heterogeneous lithosphere with varying porosities and volatile contents. Seamount subduction may impact tectonic erosion, interseismic coupling, seismogenesis, and fluid transportation (e.g., Kodaira et al., 2000; Marcaillou et al., 2016). However, the impact of hydrothermal circulation through seamounts on subduction processes

43

44

45

46

47

48

49

50

51

52

53

54

55

56

57

58

59

60

61

62

63

(Fisher & Wheat, 2010) and their role in slab hydration remain poorly understood.

In this study, we present Vp models along three trench perpendicular WAS lines spanning an ~80-km-long section of the Middle America Trench (MAT), where the ~23 Myr Cocos Plate formed at the East Pacific Rise (EPR) subducts beneath northern Costa Rica (Fig.1A&1B). Our results reveal extremely low upper mantle velocities beneath a seamount at the outer rise, which exceeds the Vp reduction to either side, indicating enhanced hydration and serpentinization at the seamount.

## **DATA AND METHODS**

We use three ridge-perpendicular WAS refraction lines to study the impact of bending-related faulting at the MAT from north to south: profiles ANE, p200e, and p50 (Fig.1A). Line p200e was collected during RRS James Cook cruise JC228 (2022/23). Thirty-seven ocean-bottom-seismometers (OBSs) were deployed along this 250-km-long profile, with collocated multibeam bathymetry, heat flow, and multi-channel seismic data (Fig.1). This line crosses a ~1.1 km high seamount at the outer rise.

To reveal the lateral structural variation of the subducting plate, we also re-examine two legacy seismic lines, ANE and p50, using the same approach and parameterization as for p200e (Fig.1A). In the north, 10 OBSs were deployed along 220-km-long line ANE in 2008, which have been used to determine mantle anisotropy (Miller et al., 2021). To the south, a 140-km-long line p50 consists of 19 stations acquired in 2003 and was analyzed by Ivandic et al. (2008).

All OBS stations recorded clear crustal refraction (Pg), Moho reflection (PmP), and upper mantle refraction (Pn) arrivals (Supplemental Material Figs.S2A-S5A, Tab.S1<sup>1</sup>). Picked

travel-times were inverted using a joint seismic refraction and reflection tomographic approach

(Korenaga et al., 2000) to generate velocity models. A Monte-Carlo method was used to test the deviation of Vp and Moho depth. For detailed information about the data collection, processing, and modeling procedures, refer to Supplemental Material.

## **COMPARISON OF VELOCITY STRUCTURES**

Overall, our results display a ~5-6 km thick incoming crust with a typical two-layer (layers 2 and 3) oceanic crustal structure at the MAT, overlain by ~500 m of sediments. Crustal thickening of 3-4 km is observed beneath the seamount crossed by line p200e (Fig.2). All three profiles display a systematic trench-ward crustal Vp reduction across the outer rise, with comparable extent and degree (Figs.2D-F, 3A). The layer 3 velocities are generally reduced by ~0.1-0.2 km/s, showing the onset of bending at ~70-80 km from the trench. However, along p200e, Vp reduction in the upper mantle is detectable ~110 km from the trench, yielding a strong anomaly with a wider extent (Figs.2D-F, 3B). The maximum upper mantle Vp reduction along p200e is ~0.6 km/s, compared to only ~0.2-0.3 km/s along lines ANE and p50.

Owing to different modeling approaches and the selection of the starting model, there are small discrepancies between the Vp results in this study and previous models (Miller et al., 2021; Ivandic et al., 2008), but the main features of the models are consistent. A detailed comparison is provided in Supplemental Material.

## **DISCUSSION**

The velocity reduction in the crust and upper mantle at the outer rise is observed in subduction zones globally and is interpreted as a result of fracturing, alteration, and hydration of the subducting plate under the bending-related tensional stress (e.g., Grevemeyer et al.,

2018; Fujie et al., 2016). Prior to subduction, the onset of Vp reduction suggests that pervasive normal faulting occurs at c.a. 70 km from the MAT offshore of northern Costa Rica (Figs.2D-F, 3A), consistent with increasing porosity caused by crustal faulting interpreted from a decreasing electrical resistivity along line ANE at 60-80 km from the MAT (Naif et al., 2015). In this region, the structural fabric of the incoming plate created at the EPR is parallel to the trench axis (Fig.1A). The reactivation of these faults may control plate deformation and bending (e.g., Ivandic et al., 2008). Both multi-channel seismic data (Ranero et al., 2003) and seismicity (Lefeldt et al., 2009) indicate that bending-related normal faulting at the MAT could extend into the upper mantle. The acceleration of hydrothermal circulation and deep percolation of seawater along the bending-related cracks and fractures significantly change the geochemical composition and water content of the subducting plate, promoting alteration to form hydrous minerals such as chlorite, amphibole, and serpentine (Christensen & Salisbury, 1975; Carlson & Miller, 2003). The upper mantle of the subducting slab is a major carrier of water into the subduction zone, affecting arc volcanism and seismogenesis (Cooper et al., 2020; van Keken et al., 2011) and, therefore, the degree of mantle serpentinization is critical to discuss the subducting water flux. Assuming that serpentinization occurs uniformly in the upper mantle and accounts for

106

107

108

109

110

111

112

113

114

115

116

117

118

119

120

121

122

123

124

125

126

Assuming that serpentinization occurs uniformly in the upper mantle and accounts for all the Vp reduction, we estimate that the maximum serpentinization along lines ANE and p50 is ~10.1% and ~8.9%, corresponding to water contents of ~1.2 wt% and ~1.1 wt%, respectively, following the equations of Carlson & Miller (2003). These values are consistent with the previous Vp results at the MAT (Grevemeyer et al., 2007, 2018), but they likely represent an

upper bound as the decrease in Vp, produced by serpentine/water filled cracks and/or wide damaged zones, is not considered (e.g., Miller & Lizarralde, 2016). Seismic anisotropy results along line ANE suggested that hydration is limited to fault zones, reducing water storage to ~0.9 wt% (Miller et al., 2021), which is lower than our estimation. Our results at the MAT reflect a moderately hydrated lithosphere of a young, hot subducting plate that has a shallow neutral plane at ~6 km below the Moho (Lefeldt et al., 2009) limiting the depth and extent of serpentinization. The southward decreasing velocity anomaly matches the decreasing dip of the subducting slab (Syracuse & Abers, 2006) and a narrowing of the area affected by bending observed in the bathymetric data (Fig.1A; Ranero et al., 2008), suggesting a systematic southward decrease of fracturing and hydration (Van Avendonk et al., 2011).

In contrast to this general trend, along profile p200e, we observe the pronounced Vp reduction of 0.2-0.6 km/s in the upper mantle underlying the seamount, which may be caused by the presence of highly serpentinization with degree of  $\sim$ 19.2% (i.e.,  $\sim$ 2.4 wt% H<sub>2</sub>O) (Figs.2B,2E,&3B). We suggest that the seamount is characterized by an increased permeability and hence facilitates the water percolation and migration during the bending process, increasing the hydration of the upper mantle (Fig.3C). Seamounts on spreading ridge flanks contribute to the crustal heat loss and fluid exchange between the oceanic lithosphere and hydrosphere due to the high porosity of extrusive volcanic edifice and volcaniclastic materials, and thin sedimentary covers (e.g., Fisher & Wheat, 2010). In our study area, extremely low heat flow (<10 mW/m<sup>2</sup>) occurs close to the seamount (HF2304 & HF2302), whereas heat flow increases to  $\sim$ 10-30 mW/m<sup>2</sup> at  $\sim$ 10 km away from the seamount (HF2303 & HF2301) and to >150

mW/m<sup>2</sup> to the south of 9°55'N (HF2309 & HF2305) (Fig.1C). Therefore, we infer that this seamount provides a recharge site for hydrothermal circulation, comparable to a similar-scale seamount, Tengosed, on the Cocos Plate away from the trench (Hutnak et al., 2008) and consequently the hydrothermal recharge in the shallow crust probably exists before bending. The seamount at p200e protrudes ~1.1 km above the surrounding seafloor, generating enough pressure difference to drive hydrothermal flow. In contrast, small seamounts or knolls may serve as discharge sites (Fisher et al., 2003), or both recharge and discharge sites (Hutnak et al., 2008), making them less supportive at supplying a continuous downward flux of seawater. The load of the volcanic edifice may lead to the flexure of the underlying oceanic plate and, therefore, may have formed fractures and faults during volcano emplacement (Fig.3C). In addition, the contact between the volcanic edifice and the neighboring oceanic crust exhibits two narrow low velocity regions of <6.5 km/s (Fig.2B), suggesting that highly fractured or altered crust surrounds the seamount which may represent important pathways for water migration (Fig.3C), although these features are not evident in bathymetry. If the water content in the upper mantle decreases linearly from ~1.2 wt% beneath line ANE to ~1.1 wt% beneath line p50, the background water content without the impact of seamount would be ~1.15 wt% along p200e; thus, the contribution of water due to the seamount is ~1.3 wt%. Our results indicate that seamounts form sites of highly increased permeability in the oceanic crust and thereby facilitate migration of large amounts of water into the upper mantle. The sporadic seamounts in the Guatemala Basin (e.g., Hutnak et al., 2008), for example, have developed a fluid-rich subducting plate, which is supported by the geochemistry of arc volcanoes (Morris

148

149

150

151

152

153

154

155

156

157

158

159

160

161

162

163

164

165

166

167

et al., 1990) and velocity anomalies in the mantle wedge and subducting slab (Syracuse et al., 2008).

169

170

171

172

173

174

175

176

177

178

179

180

181

182

183

184

185

186

187

188

189

Assuming other volcanic edifices of similar size can trap similar volumes of water, we estimate that subducting seamounts contribute ~2.2×10<sup>3</sup> Tg/Myr of water flux in the upper mantle to the deep Earth globally. This value is significantly lower than the estimation of water captured in porous volcaniclastics of the seamounts based on an electromagnetic study (5.5×10<sup>6</sup>-9.4×10<sup>6</sup> Tg/Myr; Chesley et al., 2021). This amount of water, however, cannot be neglected given its role in mantle serpentinization and its capacity to significantly modify volatile content and chemical composition in the deep mantle. Moreover, hydrated mantle, rather than crust or sediments, is a dominant supplier of subducted water to the volcanic arc as indicated by geochemical observations (Cooper et al., 2020). Additional water flux into the upper mantle caused by seamounts at trenches would greatly affect magma productivity at arcs and the genesis of intermediate-depth earthquakes by dehydration embrittlement (e.g., Cooper et al., 2020; Marcaillou et al., 2016). Note that we may have underestimated the water flux as even buried seamounts may be hydrogeologically active (Norvell et al., 2023), which can potentially be an additional source for water flux, but further geophysical evidence is needed to estimate water flux at deep beneath subducting buried seamounts.

In summary, our results reveal that seamounts efficiently increase the permeability of the oceanic crust prior to subduction, facilitate the migration of seawater into the mantle, exert control on widespread serpentinization, and notably promote water recycling back into the Earth's interior (Fig.3C). Based on the Vp reduction, we estimate that global subducting

seamounts contribute  $\sim 2.2 \times 10^3$  Tg/Myr of water flux in the upper mantle to the deep Earth.

#### **ACKNOWLEDGMENTS**

190

191

192

193

194

195

196

197

198

199

200

201

202

203

204

205

206

207

208

209

The authors thank the captain, officers, crew, and scientific party of RRS James Cook for their assistance during the cruise JC228. This research was supported by BMBF grants 03G0295OA and NERC grant NE/M021246/1. OBSs used during JC228 were provided by the UK Ocean Bottom Instrument Facility (Minshull et al, 2005) and GEOMAR. The authors thank Serge Lallemand, Susan Ellis, and one anonymous reviewer for their constructive comments. REFERENCES CITED Carlson, R. L., and Miller, D. J., 2003, Mantle wedge water contents estimated from seismic velocities in partially serpentinized peridotites: Geophysical Research Letters, v. 30, 1250, https://doi.org/10.1029/2002GL016600 Chesley, C., Naif, S., Key, K., and Bassett, D., 2021, Fluid-rich subducting topography generates anomalous forearc porosity: Nature, v. 595(7866), p. 255-260, https://doi.org/10.1038/s41586-021-03619-8 Christensen, N. I., and Salisbury, M. H., 1975, Structure and constitution of the lower oceanic crust: Reviews of Geophysics, v. 13, p. 57-86, https://doi.org/10.1029/RG013i001p00057 Cooper, G. F., Macpherson, C. G., Blundy, J. D., Maunder, B., Allen, R. W., Goes, S., ... and

the VoiLA team, 2020, Variable water input controls evolution of the Lesser Antilles

volcanic arc: Nature, v. 582, p. 525-529, https://doi.org/10.1038/s41586-020-2407-5

210	Fisher, A. T., Davis, E. E., Hutnak, M., Spiess, V., Zühlsdorff, L., Cherkaoui, A., and
211	Becker, K, 2003, Hydrothermal recharge and discharge across 50 km guided by
212	seamounts on a young ridge flank: Nature, v. 421, p. 618-621,
213	https://doi.org/10.1038/nature01352
214	Fisher, A. T., and Wheat, C. G., 2010, Seamounts as conduits for massive fluid, heat, and
215	solute fluxes on ridge flanks: Oceanography, v. 23, p. 74-87,
216	https://www.jstor.org/stable/24861064
217	Fujie, G., Kodaira, S., Sato, T., and Takahashi, T., 2016, Along-trench variations in the
218	seismic structure of the incoming Pacific plate at the outer rise of the northern Japan
219	Trench: Geophysical Research Letters, v. 43, p. 666-673,
220	https://doi.org/10.1002/2015GL067363
221	Grevemeyer, I., Ranero, C. R., Flueh, E. R., Kläschen, D., and Bialas, J., 2007, Passive and
222	active seismological study of bending-related faulting and mantle serpentinization at
223	the Middle America trench: Earth and Planetary Science Letters, v. 258, p. 528-542,
224	https://doi.org/10.1016/j.eps1.2007.04.013
225	Grevemeyer, I., Ranero, C. R., and Ivandic, M., 2018, Structure of oceanic crust and
226	serpentinization at subduction trenches: Geosphere, v. 14, p. 395-418,
227	https://doi.org/10.1130/GES01537.1
228	Harris, R. N., Fisher, A. T., and Chapman, D. S., 2004, Fluid flow through seamounts and
229	implications for global mass fluxes: Geology, v. 32, p. 725-728,
230	https://doi.org/10.1130/G20387.1

231	Hutnak, M., Fisher, A. T., Harris, R., Stein, C., Wang, K., Spinelli, G., Schindler, M.,
232	Villinger H., and Silver, E, 2008, Large heat and fluid fluxes driven through mid-plate
233	outcrops on ocean crust: Nature Geoscience, v. 1, p. 611-614,
234	https://doi.org/10.1038/ngeo264
235	Ivandic, M., Grevemeyer, I., Berhorst, A., Flueh, E. R., and McIntosh, K., 2008, Impact of
236	bending related faulting on the seismic properties of the incoming oceanic plate
237	offshore of Nicaragua: Journal of Geophysical Research: Solid Earth, v. 113,
238	https://doi.org/10.1029/2007JB005291
239	Kardell, D. A., Zhao, Z., Ramos, E. J., Estep, J., Christeson, G. L., Reece, R. S., and Hesse,
240	M. A., 2021, Hydrothermal models constrained by fine-scale seismic velocities
241	confirm hydrothermal cooling of 7–63 ma south Atlantic crust: Journal of
242	Geophysical Research: Solid Earth, v. 126(6), e2020JB021612,
243	https://doi.org/10.1029/2020JB021612
244	Kodaira, S., Takahashi, N., Nakanishi, A., Miura, S., and Kaneda, Y., 2000, Subducted
245	seamount imaged in the rupture zone of the 1946 Nankaido earthquake: Science, v.
246	289, p. 104-106, https://www.science.org/doi/full/10.1126/science.289.5476.104
247	Korenaga, J., Holbrook, W. S., Kent, G. M., Kelemen, P. B., Detrick, R. S., Larsen, H. C.,
248	Hopper, J. R. and Dahl-Jensen, T. (2000). Crustal structure of the southeast Greenland
249	margin from joint refraction and reflection seismic tomography. Journal of
250	Geophysical Research: Solid Earth, v. 105, p. 21591-21614,
251	https://doi.org/10.1029/2000JB900188

252	Lefeldt, M., Grevemeyer, I., Goßler, J., and Bialas, J., 2009, Intraplate seismicity and related
253	mantle hydration at the Nicaraguan trench outer rise: Geophysical Journal
254	International, v. 178, p. 742-752, <a href="https://doi.org/10.1111/j.1365-246X.2009.04167.x">https://doi.org/10.1111/j.1365-246X.2009.04167.x</a>
255	Li, L., Collier, J., Henstock, T., and Goes, S., 2024. Downward continued ocean bottom
256	seismometer data show continued hydrothermal evolution of mature oceanic upper
257	crust: Geology, v. 52(9), p. 717-722, <a href="https://doi.org/10.1130/G52329.1">https://doi.org/10.1130/G52329.1</a>
258	Marcaillou, B., Collot, J. Y., Ribodetti, A., d'Acremont, E., Mahamat, A. A., and Alvarado,
259	A., 2016, Seamount subduction at the North-Ecuadorian convergent margin: Effects
260	on structures, inter-seismic coupling and seismogenesis: Earth and Planetary Science
261	Letters, v. 433, p. 146-158, <a href="http://dx.doi.org/10.1016/j.epsl.2015.10.043">http://dx.doi.org/10.1016/j.epsl.2015.10.043</a>
262	Miller, N. C., and Lizarralde, D., 2016, Finite-frequency wave propagation through outer rise
263	fault zones and seismic measurements of upper mantle hydration: Geophysical
264	Research Letters, v. 43(15), p. 7982–7990, <a href="https://doi.org/10.1002/2016gl070083">https://doi.org/10.1002/2016gl070083</a>
265	Miller, N. C., Lizarralde, D., Collins, J. A., Holbrook, W. S., and Van Avendonk, H. J. A.,
266	2021, Limited Mantle Hydration by Bending Faults at the Middle America Trench:
267	Journal of Geophysical Research: Solid Earth, v. 126, e2020JB020982,
268	https://doi.org/10.1029/2020JB020982
269	Minshull, T., Sinha, M., & Peirce, C., 2005, Multi-disciplinary, sub-seabed geophysical
270	imaging - a new pool of 28 seafloor instruments in use by the United Kingdom Ocean
271	Bottom Instrument Consortium: Sea Technology, v.46, p. 27-31, <a href="https://durham-ntmax.org/learning-ntmax">https://durham-ntmax.org/learning-</a>
272	repository.worktribe.com/output/1572698

273	Morris, J. D., Leeman, W. P., and Tera, F, 1990, The subducted component in island arc lavas:
274	constraints from Be isotopes and B-Be systematics: Nature, v. 344, p. 31-36,
275	https://doi.org/10.1038/344031a0
276	Naif, S., Key, K., Constable, S., and Evans, R. L., 2015, Water-rich bending faults at the
277	Middle America Trench: Geochemistry, Geophysics, Geosystems, v. 16, p. 2582-
278	2597, https://doi.org/10.1002/2015GC005927
279	Norvell, B., Kyritz, T., Spinelli, G. A., Harris, R. N., Dickerson, K., Tréhu, A. M., et al., 2023,
280	Thermally significant fluid seepage through thick sediment on the Juan de Fuca plate
281	entering the Cascadia subduction zone: Geochemistry, Geophysics, Geosystems, v.
282	24, e2023GC010868, https://doi.org/10.1029/2023GC010868
283	Peacock, S. M., 1990, Fluid processes in subduction zones: Science, v. 248, p. 329-337,
284	https://www.science.org/doi/abs/10.1126/science.248.4953.329
285	Peacock, S. M, 2001, Are the lower planes of double seismic zones caused by serpentine
286	dehydration in subducting oceanic mantle?: Geology, v. 29, p. 299-302,
287	https://doi.org/10.1130/0091-7613(2001)029<0299:ATLPOD>2.0.CO;2
288	Ranero, C. R., Grevemeyer, I., Sahling, H., Barckhausen, U., Hensen, C., Wallmann, K.,
289	and McIntosh, K., 2008, Hydrogeological system of erosional convergent margins and
290	its influence on tectonics and interplate seismogenesis: Geochemistry, Geophysics,
291	Geosystems, v. 9, Q03S04, https://doi.org/10.1029/2007GC001679

292	Ranero, C. R., Phipps Morgan, J., McIntosh, K., and Reichert, C., 2003, Bending-related
293	faulting and mantle serpentinization at the Middle America trench: Nature, v. 425, p.
294	367-373, <a href="https://doi.org/10.1038/nature01961">https://doi.org/10.1038/nature01961</a>
295	Seton, M., Müller, R. D., Zahirovic, S., Williams, S., Wright, N. M., Cannon, J., et al., 2020,
296	A global data set of present-day oceanic crustal age and seafloor spreading
297	parameters: Geochemistry, Geophysics, Geosystems, v. 21, e2020GC009214,
298	https://doi.org/10.1029/2020GC009214
299	Syracuse, E. M., Abers, G. A., Fischer, K., MacKenzie, L., Rychert, C., Protti, M., and
300	Strauch, W., 2008, Seismic tomography and earthquake locations in the Nicaraguan
301	and Costa Rican upper mantle: Geochemistry, Geophysics, Geosystems, v. 9,
302	Q07S08, https://doi.org/10.1029/2008GC001963
303	Syracuse, E. M., and Abers, G. A., 2006, Global compilation of variations in slab depth
304	beneath arc volcanoes and implications: Geochemistry, Geophysics, Geosystems, v. 7,
305	Q05017, https://doi.org/10.1029/2005GC001045
306	Van Avendonk, H. J. A., Holbrook, W. S., Lizarralde, D., and Denyer, P., 2011, Structure
307	and serpentinization of the subducting Cocos plate offshore Nicaragua and Costa
308	Rica: Geochemistry, Geophysics, Geosystems, v. 12(6),
309	https://doi.org/10.1029/2011GC003592
310	van Keken, P. E., Hacker, B. R., Syracuse, E. M., and Abers, G. A., 2011, Subduction
311	factory: 4. Depth-dependent flux of H <sub>2</sub> O from subducting slabs worldwide: Journal of

312	Geophysical Research: Solid Earth, v. 116, B01401,
313	https://doi.org/10.1029/2010JB007922
314	Watts, A. B., Ten Brink, U. S., Buhl, P., and Brocher, T. M, 1985, A multichannel seismic
315	study of lithospheric flexure across the Hawaiian-Emperor seamount chain: Nature, v.
316	315, p. 105-111, <a href="https://doi.org/10.1038/315105a0">https://doi.org/10.1038/315105a0</a>
317	Yu, Y., Sandwell, D. T., and Dibarboure, G, 2024, Abyssal marine tectonics from the SWOT
318	mission: Science, v. 386, p. 1251-1256, <a href="https://doi.org/10.1126/science.ads4472">https://doi.org/10.1126/science.ads4472</a>
319	
320	

## 321 FIGURE CAPTIONS

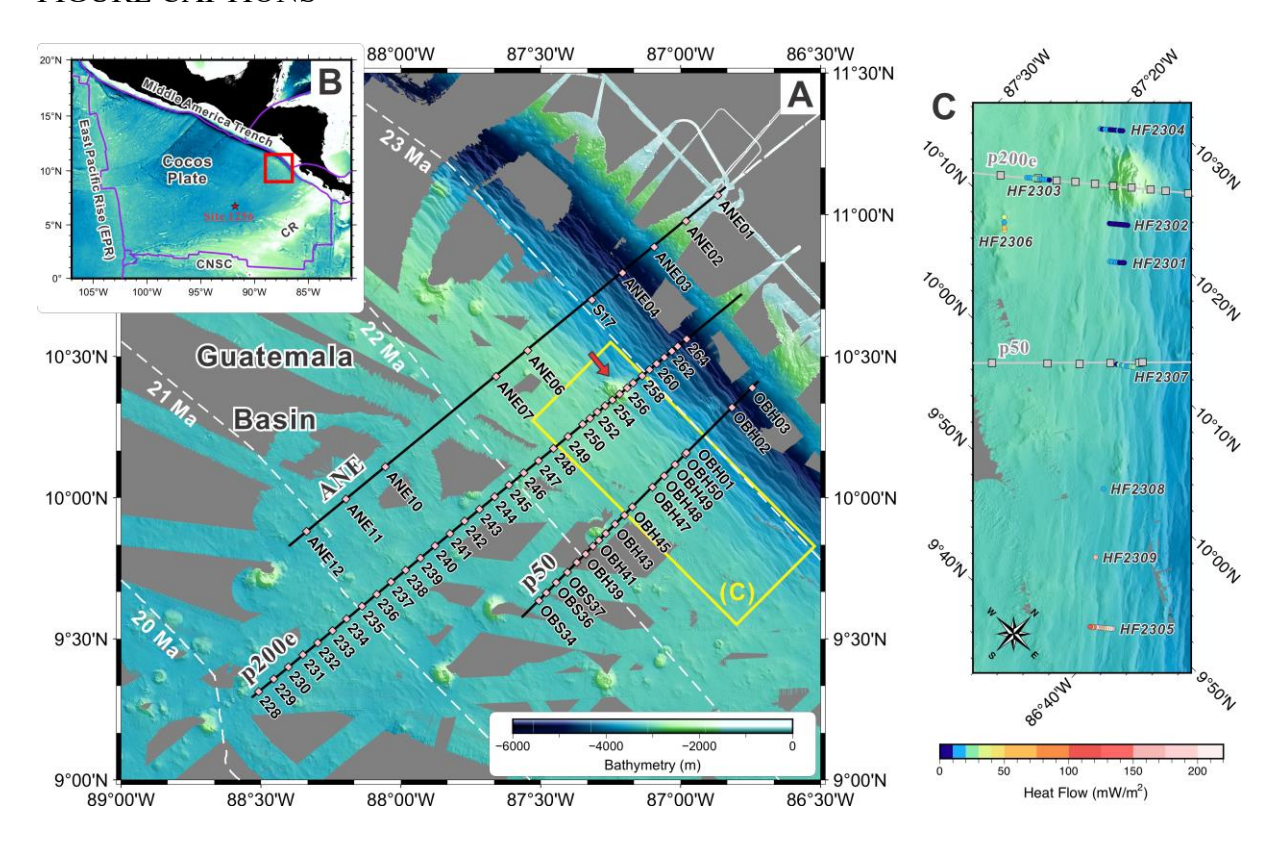


Figure 1. (A) Map of the subducting Cocos Plate and the layout of wide-angle seismic (WAS) lines. Black lines and pink rectangles show the WAS lines and the locations of ocean-bottom-seismometers, respectively. Dashed white lines are seafloor isochrons from Seton et al. (2020). The red arrow marks the seamount located at the outer rise. (B) Inset shows the Cocos Plate, with the red rectangle marking the study area in (A) and the red star indicating the position of ODP Site 1256. Purple lines are the plate boundaries. (C) Heat flow measurement area during JC228, which is marked as yellow rectangle in (A). Circles denote heat flow stations, colored by heat flow value.

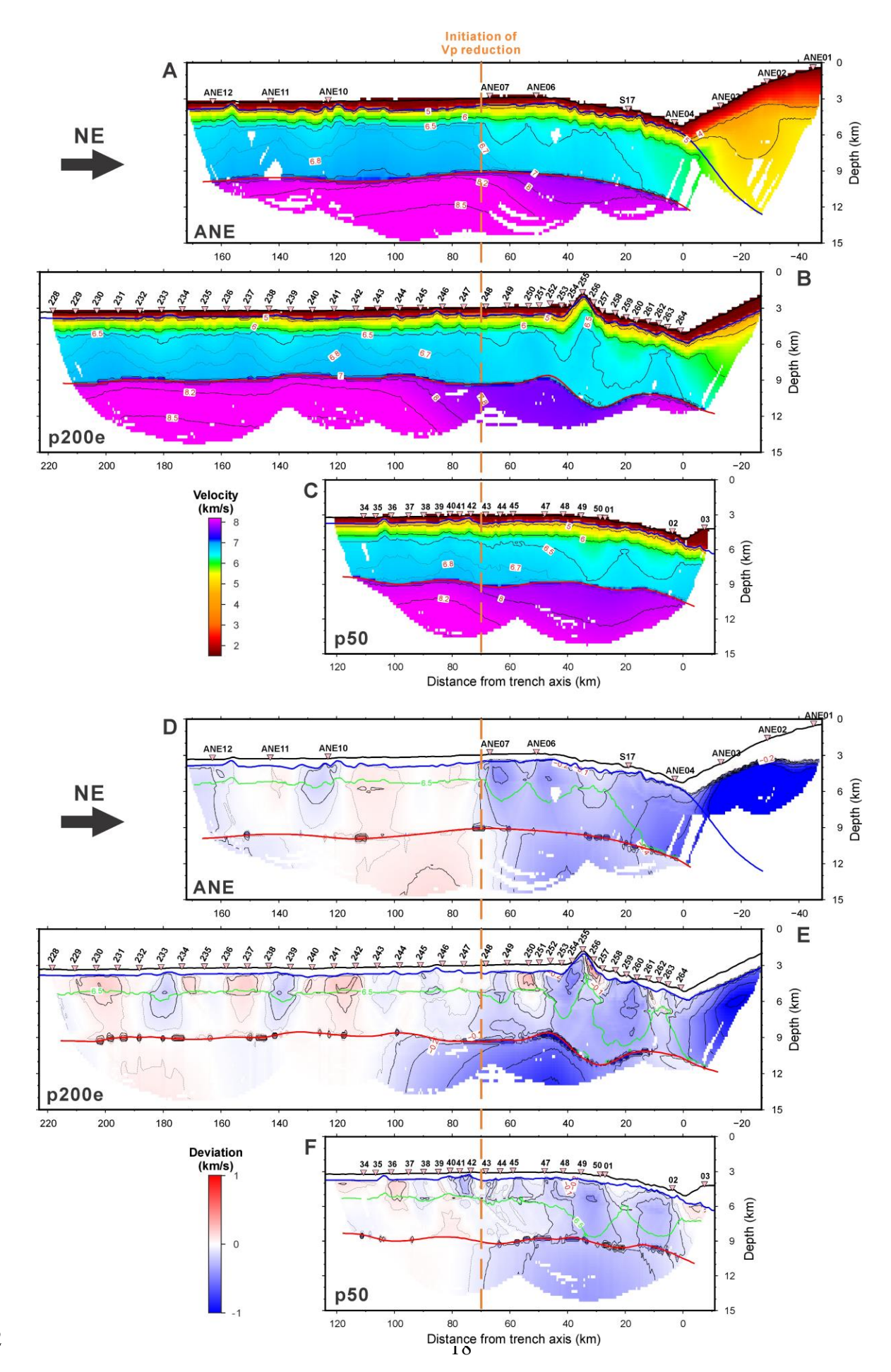


Figure 2. Results of seismic tomographic inversion. (A-C) shows the velocity structure of profiles ANE, p200e, and p50, respectively. (D-F) presents the corresponding velocity deviations that were calculated based on the reference velocity from the unaltered oceanic domain (cyan bars in A-C) along each line. The thick black, blue, red lines show the boundaries of seafloor, basement, and Moho, respectively. The dashed orange line marks the initiation of Vp reduction.

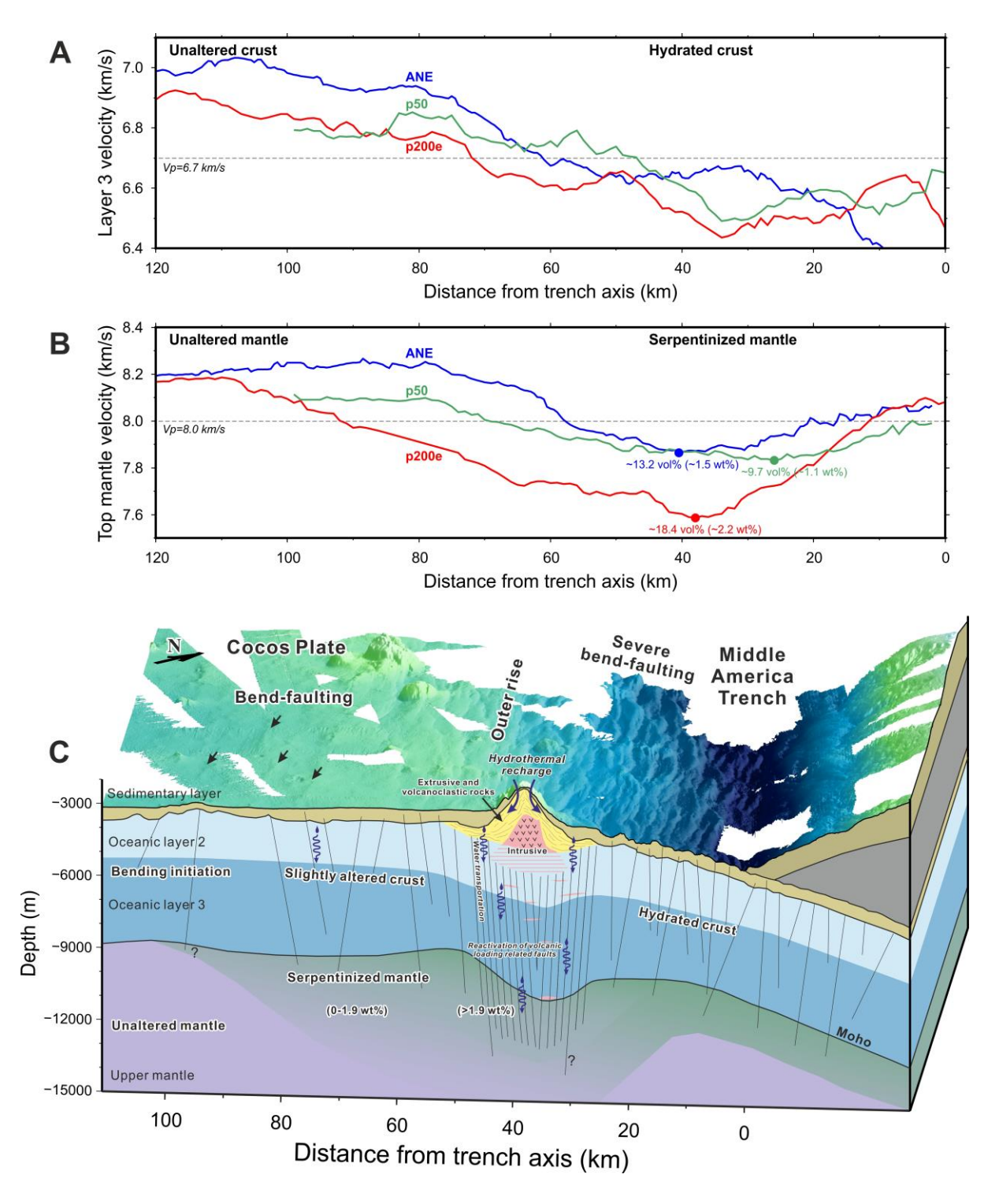


Figure 3. (A) The variation of layer 3 velocity and (B) upper mantle velocity with distance from trench axis, which are extracted from 0.5 km above and below the Moho boundary, respectively. Colored dots mark the maximum serpentinized degree (vol%) and water content (wt%) along each line estimated from Vp based on Carlson & Miller (2003). (C) 3D conceptual

model illustrating the role of the seamount at outer rise in entrainment of seawater into the crust and upper mantle. Black arrows mark the onset of bend-faulting observed from bathymetry.

1 Supplemental Material. Detailed information about heat flow data collected in cruise JC228, and data acquisition, processing, and model assessment of WAS lines p200e, ANE, and p50.

Please visit <a href="https://doi.org/10.1130/XXXX">https://doi.org/10.1130/XXXX</a> to access the supplemental material, and contact <a href="editing@geosociety.org">editing@geosociety.org</a> with any questions.